EVALUATION OF INTERFACIAL AREA TRANSPORT EQUATION IN COUPLED TWO-FLUID MODEL COMPUTATION

J.P. Schlegel*
Missouri University of Science and Technology
301 W 14th St., Rolla, MO 65401, USA
schlegelj@mst.edu

T. Hibiki
Purdue University
400 Central Dr., West Lafayette, IN 47907, USA
hibiki@purdue.edu

X. Shen
Kyoto University
2-1010, Asashiro-Nishi, Kumatori-cho, Sennan-gun, Osaka 590-0494, Japan
xzshen@rri.kyoto-u.ac.jp

S. Appathurai, H. Subramani
Chevron Energy Technology Company
1200 Smith St., Houston, TX 77002, USA
santosha@chevron.com, hjsubramani@chevron.com

ABSTRACT

The interfacial area transport equation (IATE) is an important constitutive relation for closure of the interfacial transfer terms in the two-fluid model. In spite of this, the current level of model validation for interfacial area transport models does not approach the rigor of the two-fluid model formulation. Typically the constants in the bubble coalescence and breakup kernels of the IATE are determined using a very subjective methodology. In order to provide a more rigorous and thorough benchmark of the models, a new approach is used in this paper. A full one-dimensional two-fluid model code is developed for vertical flows in large diameter channels. The code is largely based on the methodology used in TRAC-PF1/MOD2 (Spore, et al., 1993), however the interfacial drag is predicted using the interfacial drag model of Ishii and Zuber (1979). The IATE derived by Smith, et al. (2012) has been implemented. This code is then used to predict flow conditions matching the experimental data of Schlegel, et al. (2012; 2014). By making incremental changes in the various empirical constants the Hessian matrix of the IATE with respect to the many empirical constants, representing the error surface of the IATE, is numerically approximated. This allows the use of a Gauss-Newton algorithm to solve the Pareto optimization problem, when an appropriate objective function has been defined. The results of this analysis provide a rigorous mathematical and statistical basis for the benchmarked constants, in addition to a detailed sensitivity analysis for the various bubble coalescence and disintegration mechanisms.

KEYWORDS
Interfacial Area; Interfacial Transport; Pareto Optimization; Two-Fluid Model;

1. INTRODUCTION

1.1. Background and Relevance

The current generation of nuclear power plant designs are being evaluated and licensed based on the predictions of best-estimate thermal-hydraulics analysis codes. These codes are being used to computationally model the reactor system in order to determine their safety characteristics. An important component of these calculations is the prediction of the behavior two-phase mixtures, which can occur during both normal operating conditions and during accident scenarios. Prediction of two-phase mixtures is accomplished through the use of the two-fluid model. The two-fluid model treats the transport of mass, momentum and energy separately for the gas and liquid phases; for this reason it is often called the six-equation model. The equations for the individual phases are then coupled through interfacial jump conditions and interfacial transfer terms which account for interaction between the fluids at their interface. These interfacial transfer terms are generally dependent on two factors: the driving force and the surface area available for transfer to occur. The amount of surface area available per unit volume is known as the interfacial area concentration, and the importance of this quantity in two-phase flow modeling has been recognized for decades [1].

In current best-estimate codes the interfacial area concentration is predicted using algebraic correlations [2, 3]. An alternate solution was proposed by Kocamustafaogullari and Ishii [4] in the form of an Interfacial Area Transport Equation (IATE). The IATE is intended to predict the dynamic development of the interfacial structure. Since that time the formulation of the IATE has been updated and a number of bubble coalescence and breakup models have been developed for various types of channels ranging from small and large pipes to narrow rectangular channels [5-10]. Recent efforts have been made to implement one-group interfacial area transport in the system analysis code TRACE [11, 12].

One key issue in interfacial area transport modeling is the interdependence of the various models. The IATE coalescence and breakup kernels are strongly dependent on the constitutive models used in the two-fluid model. Specific constitutive models of concern are the models for interfacial drag and for the turbulent dissipation. These models play a large role in determining the void fractions and the bubble coalescence and breakup models in the IATE. In current best-estimate codes it can be difficult to substitute models for these quantities in order to quantify the effects of various models on the final prediction accuracy. A second major issue in the development of the IATE has been the subjective nature of the benchmarking efforts [5-10]. In these efforts the velocity of the gas phase and the total void fraction were calculated based on second-order least-squares curve fits. Most of the studies only included three axial measurement locations. As a result, the final IATE simulations do not ensure that mass is conserved. The simulations also may not reflect the development of the gas velocity well. The constants were then adjusted based on numerous simulations until the researcher found values that produced predictions that roughly matched the experimental data. A third major issue is that the current best-estimate thermal hydraulics analysis codes use only one gas velocity field [11, 12]. This method can produce reasonable predictions as long as the gas phase is relatively homogenous. When large variations in bubble shape and size exist, the predictions will be poor [5-10]. This is due to the differences in the transport behavior of bubbles with different sizes and shapes. These differences are illustrated in Fig. 1. On the left side of the figure the variation of bubble shape is shown, with spherical and slightly distorted bubbles being defined as the first group while cap bubbles and churn-turbulent bubbles compose the second group. These two groups are chosen based on the behavior of the drag coefficient, as shown in the right side of the figure. For this reason a two-group approach has also been proposed to improve the accuracy of the calculations [7, 13].

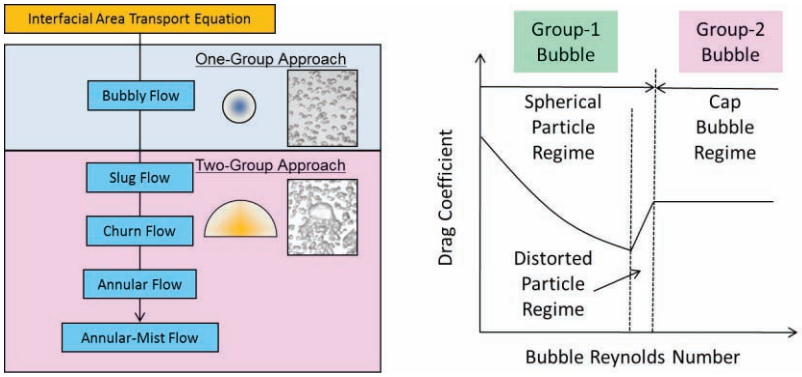

Figure 1. Illustration of the Two-Group Approach.

This paper is intended to address these three key weaknesses. The authors have written a computer script using MATLAB to dynamically solve the two-group two-fluid model coupled with a two-group IATE [14]. The calculation is simplified by assuming isothermal flow, or flow without heat transfer or mass transfer between the phases. The IATE models included in the code are applicable to flows in large diameter pipes. The code is designed to allow easy replacement of various constitutive models, specifically including (1) the IATE source and sink terms, (2) the turbulent dissipation model, and (3) the interfacial drag models. Specifically, the objectives of this paper are:

- Develop and implement an objective optimization algorithm for determining the constants in the coalescence and breakup kernels of the IATE
- Compare the results of this algorithm to previous benchmarking efforts
- Evaluate the ability of the code to predict one-dimensional interfacial area transport through comparison with experimental data

1.2. Experiment

The experimental data used for evaluating the performance of the code was collected by Schlegel et al. [15]. Experiments were performed for liquid velocities of up to 2 m/s and gas velocities up to 10.6 m/s. Measured void fractions ranged from 0.1 to 0.9. Gas injection was performed using an injector unit which allows injection of the gas as either small bubbles or as a gas jet to investigate the effect of varied inlet conditions on the flow. Experiments were performed in three separate test sections with diameters of 0.152 m, 0.203 m, and 0.304 m. Measurements were performed at three axial locations using electrical conductivity probes based on the design of Kim, et al. [16]. Benchmark experiments [16, 17] have found that the uncertainty in the local void fraction measurement is ±5%. The uncertainty in the interfacial area concentration depends on the interfacial velocity and ranges from ±5% at the lowest flow rate conditions to ±20% at the highest gas flow rate conditions.

2. TWO FLUID MODEL AND KEY CONSTITUTIVE RELATIONS

2.1. Two-Group Two-Fluid Model

The primary equations implemented in the code can be found in the work of Schlegel, et al. [14]. A brief discussion is included here.

The area-averaged two-group two-fluid model was derived by Sun, et al. [13]. This includes continuity equations for the liquid phase and the two gas fields. The momentum equations for the two gas phases are developed independently, while the liquid momentum is treated a bit differently. The actual liquid momentum equation is quite complex, involving the interfacial shear and other complex phenomena. Including all of these detailed models can make prediction of the pressure drop difficult, delay convergence, and increase the uncertainty in the result. Thus in the current study a mixture momentum equation is used to improve convergence. That equation is simplified by neglecting the time and space derivatives of the mixture momentum. The energy equations for each field are neglected in the current version of the computational tool. The two-group IATE is given by Fu and Ishii [7].

The void fraction source and sink terms and the interfacial area concentration source and sink terms are due to the interactions between bubbles resulting in coalescence or breakup. The various coalescence and breakup mechanisms for large diameter pipes are detailed by Schlegel, et al. [14]. Random collision is the impact of bubbles driven into each other by turbulent eddies. Wake entrainment occurs when a bubble is caught in the wake of a larger bubble, eventually catching up to that larger bubble and coalescing. Turbulent impact occurs when a bubble interacts with a turbulent eddy. If the turbulent eddy has enough energy to overcome the effects of surface tension, the bubble can be broken into smaller bubbles. Shearing-off occurs when a continuous stream of small bubbles is broken off from around the base of a large cap bubble due to either instabilities in the bubble surface or due to the effects of liquid shear on the skirt of the cap bubble. Surface instability occurs when small disturbances in the bubble surface grow due to the weight of the liquid above the bubble, leading to collapse in the upper surface of the bubble. Detailed models for the interfacial area and void sources and sinks for each of these models were developed by Smith, et al. [10] and implemented in the computer script used in this study. Each of these models has one or more adjustable constants designed to absorb the assumptions and simplifications involved in the derivation of each model. These constants must be determined based on benchmarking with experimental data.

2.2. Interfacial Drag and Relative Velocity

The interfacial drag terms included in the momentum equations used here are the interfacial shear, the steady-state drag, and the virtual mass force. The interfacial shear given by Ishii and Hibiki [9] relates the interfacial shear for each bubble group to the group void fractions and the wall shear. The wall shear is estimated using a two-phase friction factor model [14]. The interfacial drag for each group is calculated using the drag coefficient and relative velocity [18, 19]. The area-averaged relative velocity of each bubble group is also a challenge in a two-group model. Brooks, et al. [19] give the relative velocity for each bubble group, extending the analysis of Ishii and Mishima [20]. In these equations the area-averaging process removes the void and velocity profile information necessary to calculate the area-averaged relative velocity. This information is accounted for using correlations for the distribution parameter as recommended by Schlegel, et al. [21] for cap-bubbly and churn-turbulent flows in large diameter channels, and as recommended by Brooks, et al. [19] for bubbly flows. The asymptotic value of the distribution parameter is given by Ishii [22].

The virtual mass force accounts for the need to accelerate the liquid surrounding a bubble when the bubble velocity changes and is given by Sankaranarayanan, et al. [23]. A scaling factor f_V is approximated as being equal to one for simplicity. This approximation will not have a significant effect on the steady-state solution produced by the computational tool, but may affect the time-dependent solution.

2.3. Turbulent Dissipation

The contributions from both shear-induced and bubble-induced turbulence are accounted for in the computation. The shear-induced turbulence is approximated from the two-phase pressure drop. The bubble-induced turbulence is calculated based on the approach of Serizawa and Kataoka [24] by substituting the interfacial drag model of Ishii and Zuber [18] and accounting for two bubble groups.

2.4. Numerical Approach

The equations above are discretized using a finite volume method, with first-order upwind differencing. Two packages were prepared, one with an explicit time step and one with a semi-implicit time step. The results were compared as in Fig. 2 and it was found that the explicit time step resulting in no degradation in the accuracy of the steady-state solution, but resulted in much more rapid convergence. Here the RMS error is defined as

$$\varepsilon = \sqrt{\frac{\sum_{i=1}^{N}\left(x_{\exp} - x_{code}\right)_i^2}{N}} \tag{1}$$

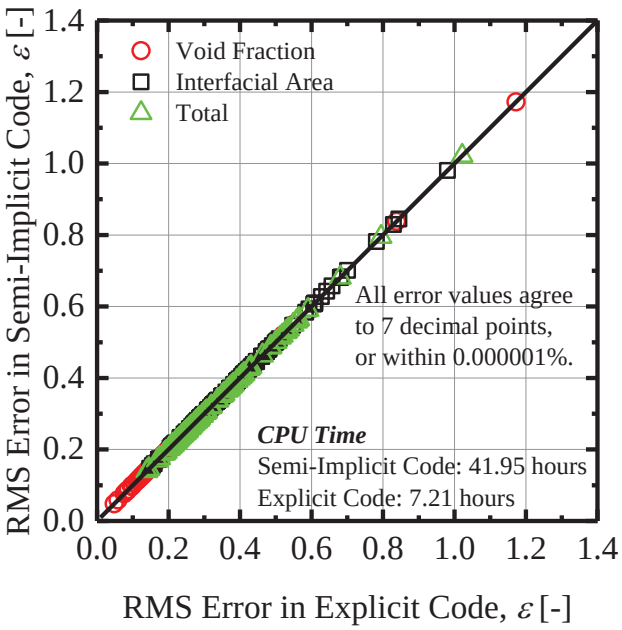

Figure 2. Error Comparison for Explicit and Semi-Implicit Solutions.

Convergence of the time-dependent solution is assumed to occur when the residual is less than 0.01. The residual in this case is defined as the maximum fractional time derivative from among the group void fractions, gas and liquid velocities, interfacial area concentrations, and pressure gradient.

3. OPTIMIZATION ALGORITHM FOR INTERFACIAL AREA TRANSPORT

The model for interfacial area transport can have significant effects on the prediction of void fraction and gas velocity through the interfacial drag laws. Predicting all of these quantities accurately amounts to a

three-objective optimization problem. There is a different optimum solution, namely a different set of 'best' benchmarked constants, for predicting each quantity. Improvement in one objective cannot generally be obtained without degradation in the other objectives. The set of solutions between the optimum values for each individual objective is known as a Pareto set, or Pareto frontier [25]. The observer determines the importance of each objective, assigning a weight value. That weight value is used to calculate a single objective function, which is then minimized to find the optimum solution. This three-objective optimization problem exists for each of the experimental tests and for each measurement location. This means that there are over 600 individual optimization problems.

To define the optimization function, some simplifications are made. Each measurement location and each experimental test are given equal weight. The importance of the gas velocity is considered to be negligible because of its strong relationship with the void fraction. The void fraction and interfacial area concentration errors are assigned equal weights. This provides an optimization function in the form:

$$F = \sqrt{\frac{\sum_{i=1}^{N}\sum_{j=1}^{2}\left(\frac{\langle\alpha\rangle_{pred,i,j} - \langle\alpha\rangle_{\exp,i,j}}{\langle\alpha\rangle_{\exp,i,j}}\right)^2 + \sum_{i=1}^{N}\sum_{j=1}^{2}\left(\frac{\langle a_i\rangle_{pred,i,j} - \langle a_i\rangle_{\exp,i,j}}{\langle a_i\rangle_{\exp,i,j}}\right)^2}{4N}} \tag{2}$$

Here N is the total number of experimental conditions. The subscript i indicates the specific experimental conditions, while the subscript j represents the measurement location. This provides a single optimization parameter for the problem.

The complex nature of the models makes it nearly impossible to develop an analytical solution to the Hessian matrix of the optimization function. The Hessian matrix is used to define the shape of the error surface and determine the direction of the change necessary for the largest decrease in the total error. To work around these issues, the following procedure is used. First an initial guess for the constants in the IATE is provided based on the work of Smith, et al. [10]. Then simulations are performed using these initial guesses. This provides the local value of the optimization function. Then each constant is varied around the initial guess and additional simulations are performed for each combination. This provides the slope of the error surface in the region surrounding the initial guess. A sample plot showing the variation in error with the change in a single adjustable constant is shown in Fig. 3. In this case, the initial value of the constant was 0.1. The plot shows that reducing this constant should decrease the objective function, as both the void fraction and interfacial area concentration minima occur at smaller constant values. However the plot also shows that the minima for the void fraction error and interfacial area concentration error occur at differing constant values – hence the need for the Pareto optimization technique.

With the error surface approximated, a Gauss-Newton algorithm is used to perform a non-linear least-squares regression. As the error surface is not linear, it is temporarily assumed to be linear in the region of the initial guess. Then the actual function is approximated as

$$f\left(\vec{x},\vec{C}\right) = f\left(\vec{x},\vec{C}^k\right) + \sum_j \frac{\partial f}{\partial C_j^k}\left(C_j^{k+1} - C_j^k\right) \tag{3}$$

which eventually leads to

$$\vec{C}^{k+1} = \vec{C}^k + \left(J^T J\right)^{-1} J^T r \tag{4}$$

where J is the Jacobian matrix, which represents an approximation of the Hessian matrix and is given by

$$J = \begin{bmatrix} \frac{\partial r_1}{\partial C_1} & \cdots & \frac{\partial r_1}{\partial C_j} \\ \vdots & \ddots & \vdots \\ \frac{\partial r_i}{\partial C_1} & \cdots & \frac{\partial r_i}{\partial C_j} \end{bmatrix} \tag{5}$$

The values of the derivatives of each residual with respect to each adjustable constant are approximated using the data from the simulations as indicated above. This process is then iterated, subject to some physical constraints, until the change in the constant values between iterations is less than 1%.

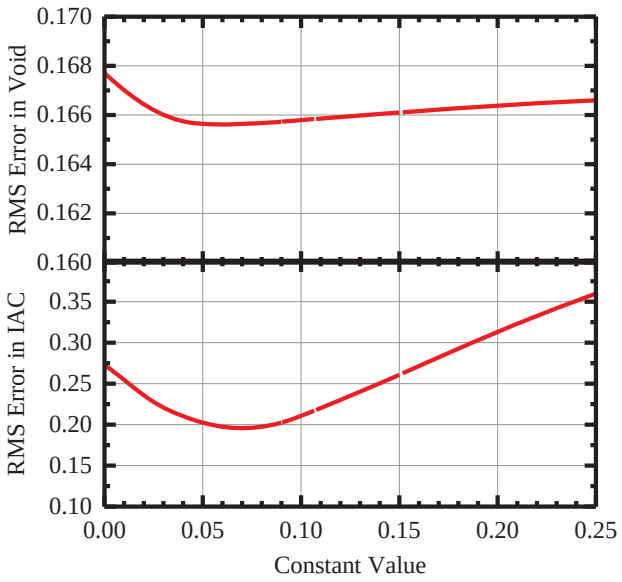

Figure 3. RMS Error as a Function of Constant Value

This method is not guaranteed to converge, due to the approximation of the Hessian matrix and elimination of the second-order derivatives. This can be mitigated somewhat using under-relaxation with appropriate bounds. Using this technique convergence can be guaranteed, however the algorithm may find a local minimum rather than a global minimum. For such complex systems with large numbers of variables, the only methods to guarantee a global minimum are stochastic. That is several random sets of initial guesses must be used, with the optimization process performed for each initial guess. Then the result with the lowest final error after convergence is used as the global minimum. Even with this process, there is a small probability that the global minimum will not be found. In addition, such efforts are very computationally intensive.

4. RESULTS AND DISCUSSION

4.1. Optimization Results

The initial guess for the Gauss-Newton algorithm described above was the constants determined by Smith, et al. [10], which are given in Table I.

Table I. Initial Guess Constants Given by Smith, et al. [10]

Constant	$C_{RC}^{(1)}$	$C_{RC,0}$	$C_{RC}^{(1,2)}$	$C_{RC,1}$	$C_{RC}^{(2)}$	$C_{RC,2}$	$C_{WE}^{(1)}$	$C_{WE}^{(1,2)}$	$C_{WE}^{(2)}$	$C_{TI}^{(1)}$	$We_{cr,1}$	$C_{TI}^{(2,1)}$	$C_{TI}^{(2)}$	$We_{cr,2}$	C_{SO}	We_{gc}	$We_{cr,SO}$	C	$\alpha_{\max}$
Value	0.01	3.0	0.01	3.00	0.01	3.00	0.002	0.01	0.06	0.050	1.20	0.04	0.01	1.20	$2.5\cdot10^{-6}$	1.20	4000	1.0	0.62

Several of these constants are not actually empirical constants. Their value was derived either through analytical considerations or through the work of previous researchers. These constants are shown in Table II. The critical Weber number given by Smith, et al. [10] is based on previous research into bubble breakup. The maximum-packing void fraction is calculated as the maximum packing of solid spheres in a tetrahedral lattice.

Table II. Physical Constants

Constant	$We_{cr,1}$	$We_{cr,2}$	We_{gc}	$\alpha_{\max}$
Value	1.20	1.20	1.20	0.74

Of the remaining constants, several approached zero very early in the optimization process, and remained there. These include the constants in the random collision models for Group 2 and the turbulent breakup model for Group 2. It is hypothesized that this is due to the very small number density of Group 2 bubbles, which would result in very little random interaction between them. Associated with the random collision model are coalescence efficiency constants, which no longer have meaning if the model constants are zero. These are listed in Table III.

Table III. Constants with an Optimized Value of Zero

Constant	$C_{RC}^{(1,2)}$	$C_{RC,1}$	$C_{RC}^{(2)}$	$C_{RC,2}$	$C_{TI}^{(2)}$
Value	0.00	3.00	0.00	3.00	0.00

This leaves a total of ten non-zero optimized constants. These constants are listed in Table IV. By comparison with the constants given for the initial guess in Table I, several conclusions can be drawn. First, the Group 1 constants tend to be slightly higher in the new benchmark. This is indicative on the dominance of the Group 1 coalescence and breakup effects on the total interfacial area concentration. However of particular interest are the large increases in the wake entrainment constants for Group 2 and the shearing-off constant. This indicates that these mechanisms may be much more important for the prediction of interfacial area concentration than originally estimated.

Table IV. Optimized Constants

Constant	$C_{RC}^{(1)}$	$C_{RC,0}$	$C_{WE}^{(1)}$	$C_{WE}^{(1,2)}$	$C_{WE}^{(2)}$	$C_{TI}^{(1)}$	$C_{TI}^{(2,1)}$	C_{SO}	$We_{cr,SO}$	C
Value	0.02	3.0	0.019	0.15	0.15	0.095	0.04	$1\cdot10^{-4}$	1.01	1.0

4.2. Prediction Accuracy

The optimization process described above has reduced the RMS average error in the interfacial area concentration predictions from 52.3% to 34.9%. This represents a significant improvement in the ability of the two-fluid model, coupled with the IATE, to predict this data set.

The computational tool was also used to predict the void fraction development for a number of low void fraction data sets collected in the transition between bubbly and cap-bubbly flow by Shen, et al. [26]. These conditions test the ability of the code to predict the creation of Group 2 bubbles and the resulting flow regime transition from a mixture that begins as a relatively homogenous bubbly flow. The results using both the previous and new benchmark constants are shown in Fig. 4 for a selection of the conditions tested. The experimental facility in this case had a diameter of 0.20 m and a total length of 26 m, and

only the area-averaged void fraction was reported. Figures 4(a) and 4(b) show flow conditions that begin in dispersed bubbly flow at the inlet to the test facility. The plots show the effect of the changes in the bubble coalescence behaviors, as the new predictions show significantly smaller Group 2 void fractions and larger Group 1 void fractions. This is expected in this region. Figure 4(b) does indicate that the code does not predict the transition to cap-bubbly flow very well at low void fractions, which highlights the need for additional detailed benchmarking data at low liquid flow rates and low void fractions. Figures 4(c) and 4(d) show the transition to cap bubbly flow for injection conditions at higher void fraction, very near the predicted flow regime transition. In both experiments the bubbles are introduced as a reasonably homogenous bubbly flow, which quickly transitions to cap-bubbly flow due to bubble coalescence. In both cases the location where transfer of the gas phase from Group 1 to Group 2 begins, the flow regime transition, is very well-predicted. The long-term behavior of the void

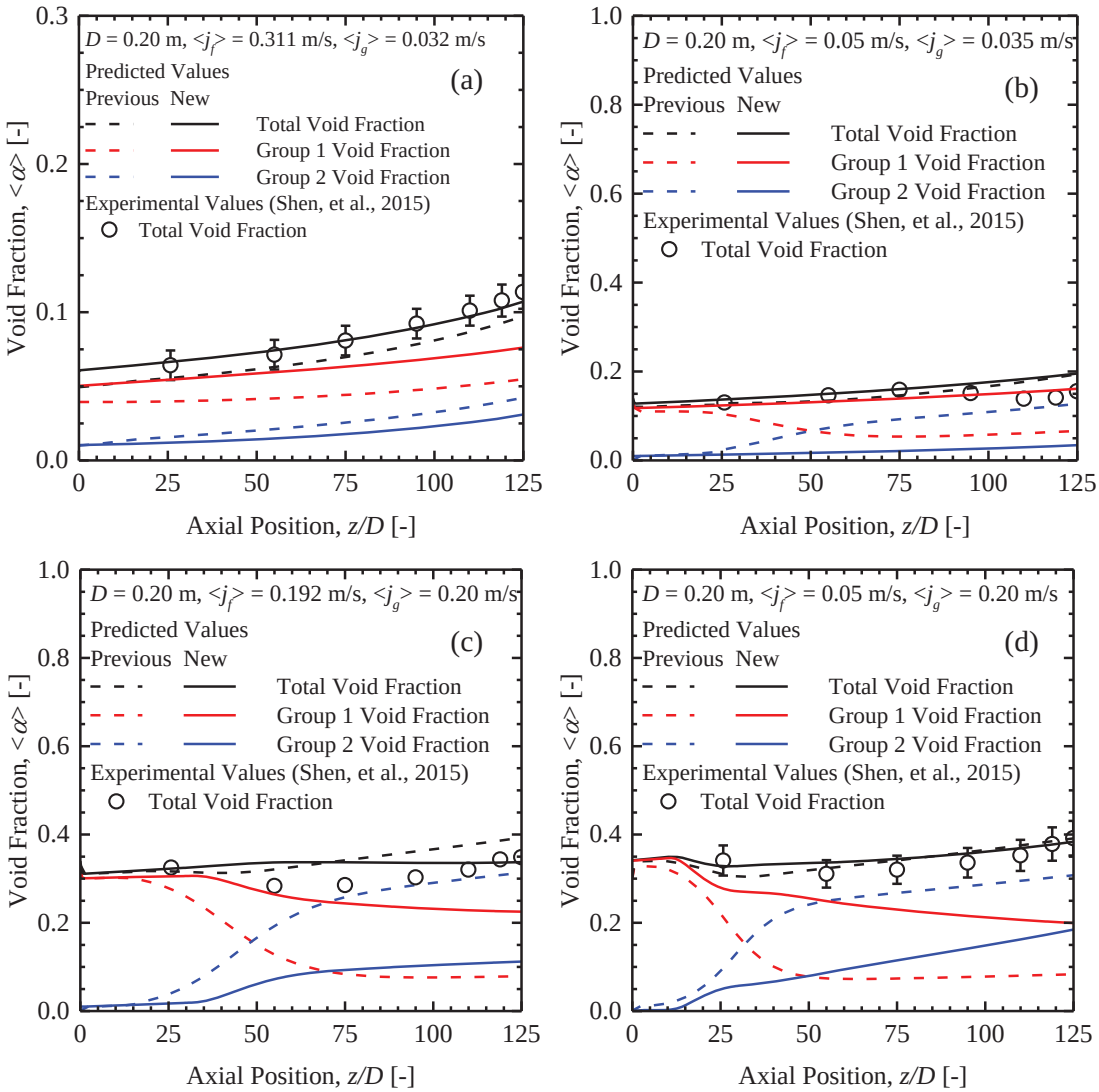

Figure 4. Comparison of Code Prediction with Data of Shen, et al. [26]

distribution between the groups is also much more realistic using the new constants. In some cases however, the decrease in the total void fraction due to this transition is either less apparent or not predicted at all. This indicates some possible shortcomings in the models for interfacial drag, especially for Group 2 bubbles. This is a shortcoming that should be addressed in future work.

In addition to the ability of the model to predict the transition between flow regimes, the ability to accurately predict interfacial area concentration must be demonstrated. Figure 5 shows a selection of flow conditions predicted at varying liquid flow rates and void fractions in order to illustrate the variation of the flow behavior with these conditions. The void fractions range from 0.1 to 0.9. The exact conditions for void fraction and interfacial area condition were provided at the inlet along with the total gas flow rate, then the code calculated the inlet gas velocities based on those inputs in order to preserve the mass flow rate of the gas.

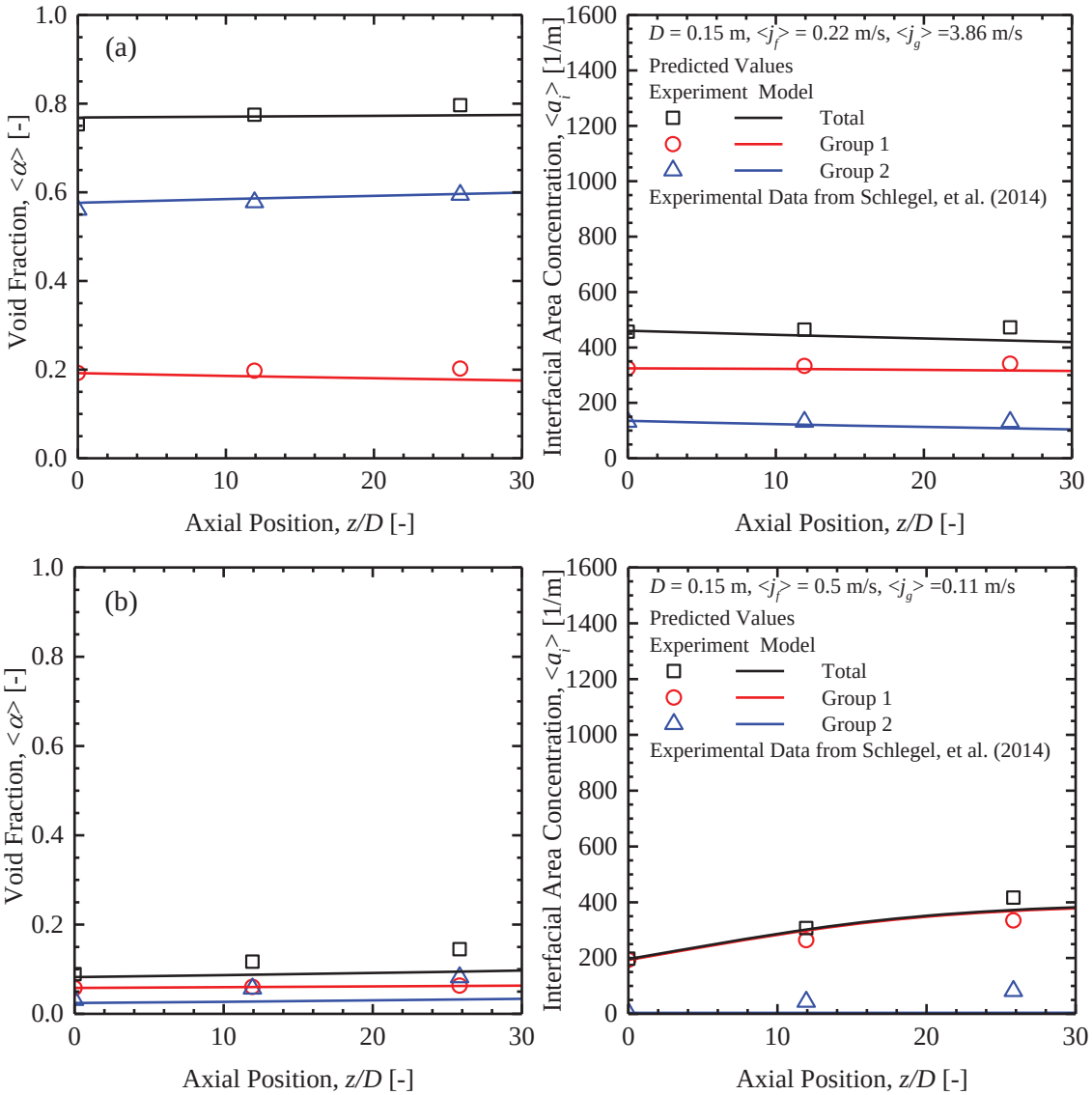

Figure 5(a-b). Comparison of Code Prediction with Data of Schlegel, et al. [15]

At very high void fractions such as Fig. 5(a), the dominance of coalescence mechanisms results in a decrease in the interfacial area concentration along the test section. This is largely driven by coalescence of Group 2 bubbles, while the Group 1 bubbles remain in equilibrium. At very low void fractions such as those in Fig. 5(b) turbulent breakup of Group 1 bubbles is the dominant bubble interaction mechanism, as indicated by the increasing interfacial area concentration along the test facility. As with the plots in Fig. 4, this plot also indicates that the current models have great difficulty in predicting the behavior of Group 2 bubbles when the void fraction is small. This supports the need for additional analysis of the interfacial drag and coalescence and breakup models for Group 2 under these conditions.

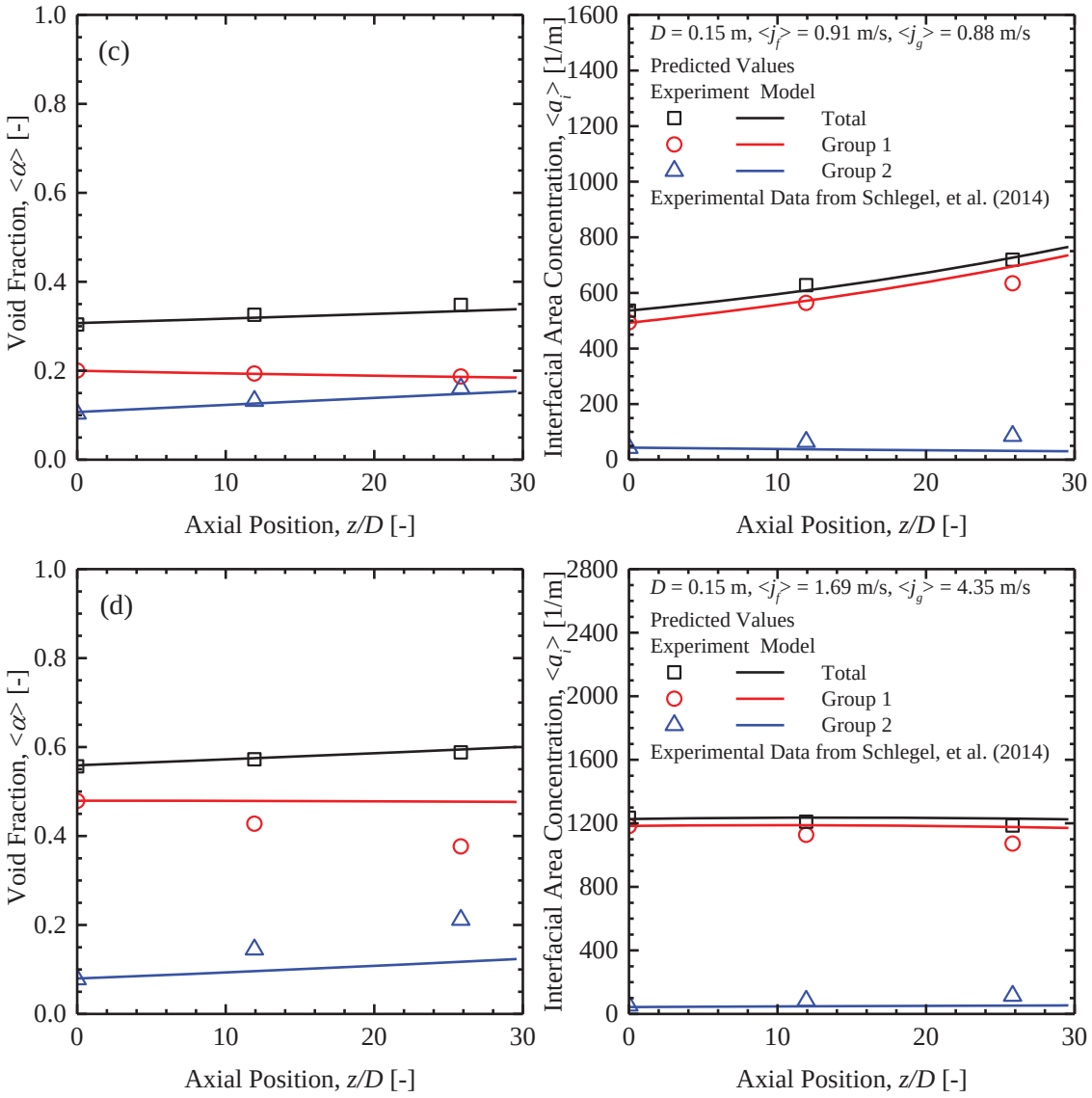

Figure 5(c-d). Comparison of Code Prediction with Data of Schlegel, et al. [15]

Figure 5(c) shows that at intermediate values the interfacial area concentration behavior is dominated by the expansion and breakup of Group 1 bubbles, while the void fraction is slowly transferred from Group 1 to Group 2 by expansion and bubble coalescence. The data also shows that as the liquid flow rate

increases, the resulting increase in turbulence results in the Group 1 void fraction representing a higher percentage of the total void fraction. Figure 5(d) shows that as the void fraction continues to increase that the competition between coalescence and breakup results in very little change in the interfacial area concentration, however part of the reason for this is that the bubble residence time in the test section is very small at such high mixture velocities. This means that the bubbles do not have very long to interact by coalescence and breakup, so the changes in interfacial area concentration along the test section will remain small.

It should also be noted that the prediction error for the total void fraction can be quite large when the liquid velocity is small. This is especially noticeable in some of the simulation results for conditions with a nominal liquid velocity of 0.25 m/s. This is due to uncertainties in the interfacial drag, which have a much larger effect on the void fraction prediction at low liquid velocities. As a result, the void fraction can be difficult to accurately predict under those conditions.

The results presented here highlight distinct needs for improvement in two areas. First is a need for high-quality experimental data including measurements of void fraction, interfacial area concentration, and gas velocity at multiple axial locations to provide a more thorough database for benchmarking the interfacial area transport models. The second is a need for improved modeling of the interfacial drag for large cap bubbles under low void fraction conditions. The data indicates that the interfacial drag may be over-predicted under these conditions.

5. CONCLUSIONS

Experimental data collected by Shen, et al. [26] and Schlegel, et al. [15] has been used to optimize and evaluate a computational tool to predict flow development in large diameter channels using a three-field two-fluid model coupled to a two-group interfacial area transport equation. A new objective optimization technique based on Pareto optimization and a Gauss-Newton iterative solution algorithm was developed and used to determine the optimum coefficients for the bubble breakup and coalescence kernels in the interfacial area transport source and sink terms.

- Overall prediction error for the interfacial area concentration was reduced from 52.3% to 34.9% using the new optimization technique.
- The prediction improvement was more pronounced for higher liquid velocity conditions, where errors in the interfacial drag models have less significant effects.
- The code is able to predict many features of the transition from bubbly to cap/slug flow, although uncertainties in the interfacial drag models create some inaccuracies.
- Additional experimental research is needed to provide more high-quality experimental data for further optimization and benchmarking efforts
- Interfacial drag models for cap bubbles should be investigated, especially at low void fractions and low liquid flow rates.

The computational tool will continue to be improved. Implementation of a fourth set of field equations representing droplets is planned. This will necessitate the implementation of droplet entrainment and deposition models as well as new interfacial drag laws, but should improve the ability of the code to predict very high void fraction conditions in annular flows.

REFERENCES

1. K. Akita and F. Yoshida, "Bubble Size, Interfacial Area, and Liquid-Phase Mass Transfer Coefficient in Bubble Columns," *Ind. Eng. Chem. Process Des. Develop.* **13**, pp. 84-91 (1974).
2. J.W. Spore, S.J. Jolly-Woodruff, T.K. Knight, J.C. Lin, R.A. Nelson, K.O. Pasamehmetoglu, R.G. Steinke, and C. Unal, *TRAC-PF1/MOD2, vol. 1: Theory Manual*, LA-12031-M, vol. I, NUREG/CR-5673, USA (1993).
3. Thermal Hydraulics Group, *Relap5/Mod3 Code Manual. Vol. I: Code Structure, System Models and Solution Methods*, RELAP5/MOD3.2.2Beta, USA (1998).
4. G. Kocamustafaogullari and M. Ishii, "Foundation of the interfacial area transport equation and its closure relations," *Int. J. Heat Mass Transfer* **38**, pp. 481-493 (1995).
5. Q. Wu, S. Kim, M. Ishii, and S.G. Beus, "One-group interfacial area transport in vertical bubbly flow," *Int. J. Heat Mass Transfer* **41**, pp. 1109–1112 (1998).
6. X. Sun, S. Kim, M. Ishii, and S. G. Beus, "Modeling of bubble coalescence and disintegration in confined upward two-phase flow," *Nucl. Eng. Des.* **230**, pp. 3-26 (2004).
7. X. Y. Fu and M. Ishii, "Two-group interfacial area transport in vertical air-water flow: I. Mechanistic model," *Nucl. Eng. Des.* **219**, pp. 143-168 (2003).
8. T. Hibiki and M. Ishii, "Interfacial area concentration of bubbly flow systems," *Chem. Eng. Sci.* **57**, pp. 3967–3977 (2002).
9. M. Ishii and T. Hibiki, *Thermo-fluid dynamics of two-phase flow, 2nd edition*, Springer, New York (2010).
10. T. R. Smith, J. P. Schlegel, T. Hibiki, and M. Ishii, "Mechanistic modeling of interfacial area transport in large diameter pipes," *Int. J. Multiphase Flow* **47**, pp. 1-16 (2012).
11. J.D. Talley, S. Kim, J. Mahaffy, S.M. Bajorek, and K. Tien. "Implementation and evaluation of one-group interfacial area transport equation in TRACE," *Nucl. Eng. Des.* **241**, pp. 865-873 (2011).
12. J.D. Talley, T. Worosz, S. Kim, S.M. Bajorek, and K. Tien. "Effect of bubble interactions on the prediction of interfacial area in TRACE," *Nucl. Eng. Des.* **264**, pp. 134-145 (2013).
13. X. Sun, M. Ishii, and J. M. Kelly, "Modified two-fluid model for the two-group interfacial area transport equation," *Annals of Nuclear Energy* **30**, pp. 1601-1622 (2003).
14. J.P. Schlegel, T. Hibiki, M. Ishii, X. Shen and S. Appathurai. "Implementation of Two-Group Interfacial Area Transport in a One-Dimensional Computational Environment," *Proceedings of the International Topical Meeting on Advances in Thermal Hydraulics 2014 (ATH '14)*, Reno, Nevada, USA (2014).
15. J.P. Schlegel, S. Sharma, R.M. Cuenca, T. Hibiki, and M. Ishii. "Local Flow Structure Beyond Bubbly Flow in Large Diameter Channels," *Int. J. Heat Fluid Flow* **47**, pp. 42-56 (2014).
16. S. Kim, X.Y. Fu, X. Wang, and M. Ishii. "Development of the miniaturized four-sensor conductivity probe and the signal processing scheme," *Int. J. Heat Mass Transfer* **43**, pp. 4101-4118 (2000).
17. A. Manera, B. Ozar, S. Paranjape, M. Ishii and H.M. Prasser, "Comparison between wire-mesh sensors and conductive needle-probes for measurements of two-phase flow parameters," *Nucl. Eng. Des.* **239**, pp. 1718-1724 (2009).
18. M. Ishii and N. Zuber, "Drag coefficient and relative velocity in bubbly, droplet or particulate flows," *AIChE Journal* **25**, pp. 843-855 (1979).

19. C. S. Brooks, S. S. Paranjape, B. Ozar, T. Hibiki, and M. Ishii. "Two-group drift-flux model for closure of the modified two-fluid model," *Int. J. Heat Fluid Flow* **37**, pp. 196-208 (2012).
20. M. Ishii and K. Mishima, "Two-fluid model and hydrodynamic constitutive relations," *Nucl. Eng. Des.* **82**, pp. 107-126 (1984).
21. J.P. Schlegel, C. Macke, T. Hibiki, and M. Ishii. "Modified Distribution Parameter for Churn-Turbulent Flow in Large Diameter Channels," *Nucl. Eng. Des.* **263**, pp. 138-150 (2013).
22. M. Ishii, *One-dimensional drift–flux model and constitutive equations for relative motion between phases in various two-phase flow regimes*, ANL-77-47, USA (1977).
23. K. Sankaranarayanan, S. Shan, I.G. Kevrekidis, and S. Sundaresan, "Analysis of drag and virtual mass forces in bubbly suspensions using an implicit formulation of the lattice Boltzmann method," *Journal of Fluid Mechanics* **452**, pp 61-96 (2002).
24. A Serizawa and I. Kataoka, "Turbulence suppression in bubbly two-phase flow," *Nucl. Eng. Des.* **122**, pp. 1-16 (1990).
25. C. Coello, G.B. Lamont, and D.A. van Veldhuizen. *Evolutionary Algorithms for Solving Multi-Objective Problems,* Springer Science & Business Media, New York (2007).
26. X. Shen, T. Hibiki, and H. Nakamura, "Bubbly-to-cap bubbly flow transition in a long-26m vertical large diameter pipe at low liquid flow rate," *Int. J. Heat Fluid Flow* **52**, pp. 140-155 (2015).